Obstacle Test for Large Deformation Plasticity Problems

Jeffrey Heckman

Lockheed Martin Corporation

Jacob Fish

Department of Mechanical, Aerospace and Nuclear Engineering

Rensselaer Polytechnic Institute

ABSTRACT

An obstacle test for large deformation plasticity problems is proposed for evaluation of mathematical models and numerical algorithms. The obstacle test consists of a suite of verification and validation problems. We evaluate performance of several well known hypoelastic and hyperelastic models in the obstacle test. Among the hypoelastic formulations we consider those based on Jaumann and Green Naghdi objective stress rates. The two hyperelastic formulations evaluated are those of Simo *et. al*. [8, 9,10] and Eterovic and Bathe [11]. We report several interesting anomalies.

1. INTRODUCTION

Over the past four decades modeling and simulation of materials undergoing large deformation plasticity has been a much researched area in computational mechanics community. Numerous mathematical models and corresponding algorithms appeared in the open literature. Yet, these models and algorithms are often compared with other so-called "established" models and algorithms. While there are some general guidelines for verification and validation [24], to our knowledge there is no established procedure to evaluate the quality of large deformation plasticity models including inelastic material response, decomposition of elastic and inelastic deformation, rotational and material stress update algorithms.

In this manuscript, an obstacle test for finite deformation plasticity problems is proposed and several well-known models are tested in the obstacle test. The proposed obstacle test consists of three categories of test problems: (i) qualitative verification, (ii) quantitative verification and (iii) validation. The qualitative verification problems are those where certain characteristics of the solution are known, such as for instance stress is expected to monotonically increase (or decrease) with deformation. Quantitative verification problems are those for which an analytical solution is available. Finally, validation problems are those for which experimental data exists. Two hypoelastic algorithms, employing the well-known Jaumann and Green-Naghdi objective stress rates, and two hyperelastic algorithms, Simo et. al. [8, 9, 10] and Eterovic and Bathe [11], were tested in the obstacle test. The choice of these algorithms was arbitrary; by no means is it implied that these are the best algorithms available in the literature. Prior to testing these algorithms in the obstacle test we reproduced the published results to ensure proper implementation. We do not identify the source of error (whether it is due to material response, large rotations, decomposition of elastic and inelastic response, etc.) except that we ensure that the error is neither due to finite element discretization nor due to excessive load step. For all test problems considered finite element meshes were taken to be sufficiently fine to ensure that the discretization errors were negligible and load increment were taken to be sufficiently small to ensure accurate integration of stresses.

2. THE OBSTACLE TEST

The proposed obstacle test consists of three categories of test problems: (i) a qualitative verification problem, (ii) quantitative verification problems and (iii) validation problems. The uniform isochoric deformations simple shear problem is a single qualitative verification problem selected. The two quantitative verification problems are the perfectly plastic thick walled cylinder and the thick walled sphere with isotropic exponential hardening. The three validation problems are: the tensile test, ball bearing forging, and upsetting of a cylindrical billet.

2.1 Definition of a Qualitative Verification Problem

The uniform isochoric deformation simple shear problem is often used for verification and validation of numerical algorithms. To our knowledge there is no analytical solution or experimental data available, but certain trends of the solution have been experimentally observed. The uniform isochoric deformation problem can be easily simulated because it consists of a single material point and does not require finite element analysis. Material properties used for the simple shear problem are summarized in Table 1.

Table 1: Material Properties for Simple Shear

Shear Modulus, μ	76.92 MPa
Bulk Modulus, K	166.67 MPa
Initial Yield Strength $Y\big\vert_{\tilde{\varepsilon}^p=0}$	0.75 MPa
Hardening, H	2.0 MPa
Hardening Parameter, β β=1 –––>Isotropic Hardening β=0 –––>Kinematic Hardening	0 or 1

The following deformation gradient describes an isochoric simple shear deformation.

$$\underset{\sim}{F} = \begin{bmatrix} 1 & t & 0 \\ 0 & 1 & 0 \\ 0 & 0 & 1 \end{bmatrix} \quad t \in [0,6] \tag{2.6}$$

Such a deformation gradient can be simulated experimentally with fixed end torsion of a hollow cylinder. This seemingly simple deformation created much debate in the scientific community. The exact solution for this test problem is unknown, but certain trends of the solution have been observed. For instance, Nagtegaal and deJong [12] and Montheillet et. al [13] presented experimental results for torsion testing of metals. For aluminum and α-iron, the torsion (shear stress) rose to a peak value and then decreased slightly, approaching a positive constant value of shear stress for large shear strain. Small oscillations of diminishing amplitude were observed for copper [13], before approaching a constant value of shear stress at large shear strain. Axial compression was observed during torsion with a local maximum value occurring when the shear stress was a maximum. Swift [14] investigated seven metals subjected to unconstrained torsion and found that the specimens elongated. Therefore, compressive, axial stress is expected for constrained torsion, supporting the experimental results of [13]. A qualitative representation of the experimental results of [13] is shown in Figure 1. For the axial stress, Figure 1 depicts a bifurcation point following the initial maximum compressive value after which the axial stress becomes either compressive or tensile.

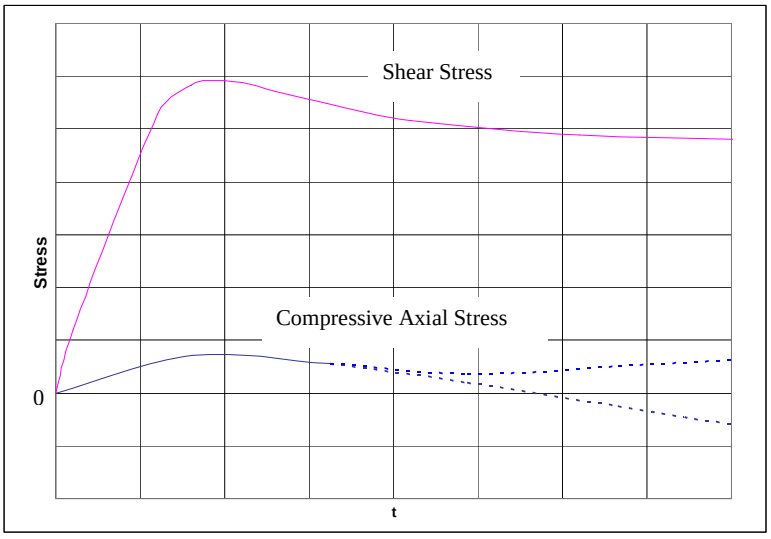

Figure 1: Qualitative Stress Response for Simple Shear

2.2 Definition of Quantitative Verification Problems

2.2.1 Expansion of a Thick-Walled Cylinder

An analytical solution of pressure distribution in a thick-walled cylinder subjected to internal pressure has been given in [19]. The cylinder, with an inner radius of 10 units and an outer radius of 20 units, is subjected to internal pressure as shown in Figure 2.

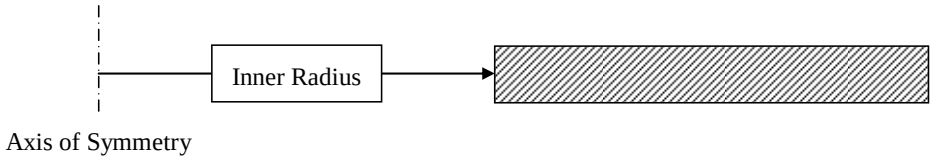

Figure 2 Geometry of a Thick-Walled Cylinder

The material is modeled as elastic perfectly plastic; material properties are given in Table 2.

Table 2: Material Properties for Thick-Walled Cylinder

Shear Modulus, μ	76.92 MPa
Bulk Modulus, K	166.67 MPa
Initial Yield Strength $Y\big\|_{\bar{\varepsilon}^p=0}$	0.75 MPa

The inner radius is driven to a value of 85 units. The analytical solution of the radial Cauchy stress, σ_{rr}, at the inner boundary vs. current inner radius is shown in Figure 3.

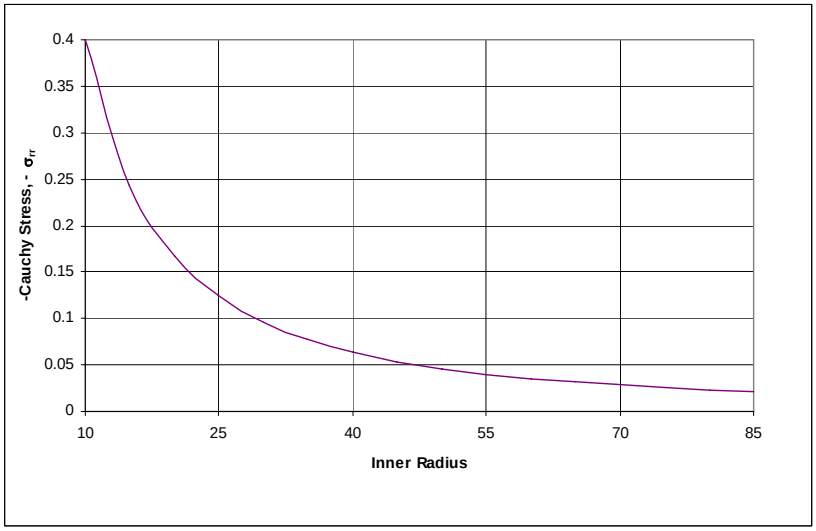

Figure 3: Analytical Solution of Inner Boundary Cauchy Radial Stress, σ_{rr}, vs. Inner Radius

2.2.2 Expansion of a Thick-Walled Sphere

An analytical solution of pressure distribution in a thick-wall sphere subjected to internal pressure has been given in [20]. The initial inner radius, a_0, and outer radius, b_0, 12.5 mm and 20 mm, respectively, were considered. An axisymmetric 7.5 degree slice of the sphere is shown in Figure 4.

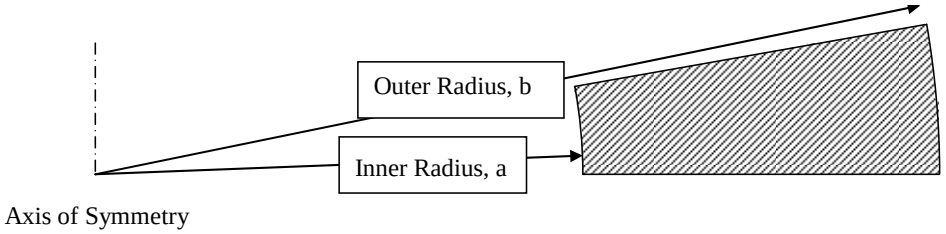

Figure 4: Initial Geometry of Thick-Walled Hollow Sphere

The material is modeled using nonlinear isotropic hardening law:

$$Y\left(\tilde{\varepsilon}^{p}\right) = Y\big|_{\tilde{\varepsilon}^{p}=0} + \left(Y_{\infty} - Y\big|_{\tilde{\varepsilon}^{p}=0}\right)\left(1 - e^{\left(-\delta\tilde{\varepsilon}^{p}\right)}\right) \tag{2.7}$$

with material properties summarized in Table 3.

Table 3: Material Properties for Thick-Walled Sphere

Shear Modulus, μ	300 MPa
Bulk Modulus, K	8000 MPa
Initial Yield Strength $Y\big\|_{\tilde{\varepsilon}^p=0}$	0.083 MPa
Saturation Yield Strength, Y_∞	0.456 MPa

The elastic constants are chosen to model incompressible material [20]. The inner radius is driven to a value of 20 mm. The analytical results of pressure versus porosity of the sphere are given in Figure 5.

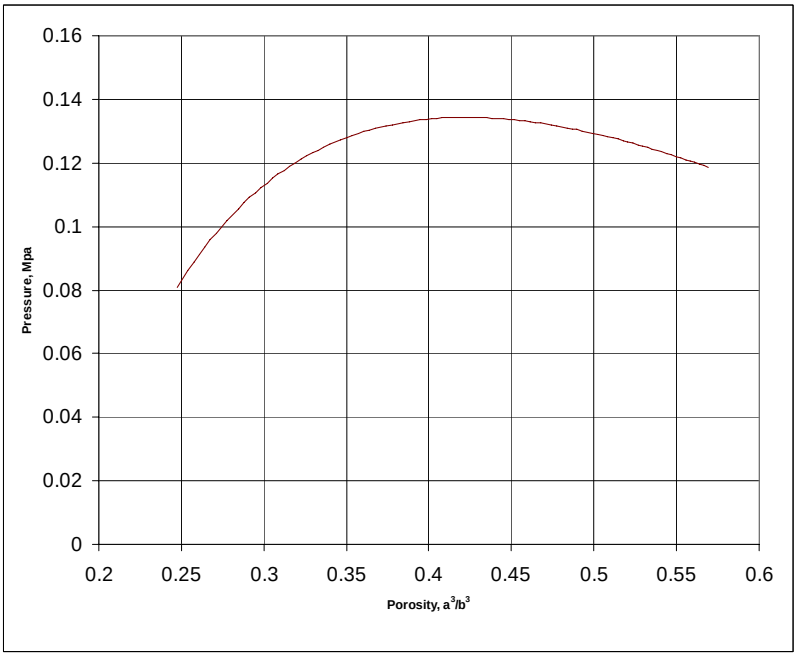

Figure 5: Internal Pressure vs. Porosity for Thick-Walled Sphere

2.3 Definition of Validation Problems

2.3.1 Necking of Circular Bar

The necking of a circular bar resulting from uniaxial tension was reported in [**Error! Reference source not found.**]. The circular bar specimen has a radius of 6.413 mm and length of 53.334 mm as shown in Figure 6.

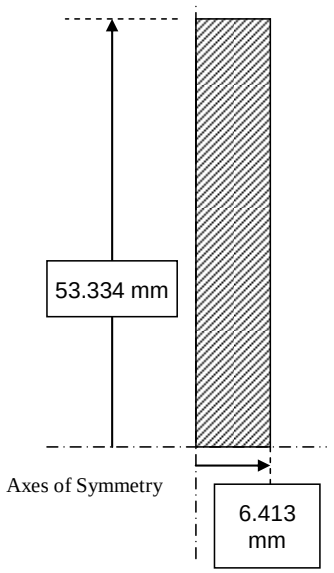

Figure 6: Initial Geometry of Circular Bar

A nonlinear isotropic hardening law

$$Y\left(\tilde{\varepsilon}^{p}\right)=Y\big|_{\tilde{\varepsilon}^{p}=0}+H\tilde{\varepsilon}^{p}+\left(Y_{\infty}-Y\big|_{\tilde{\varepsilon}^{p}=0}\right)\left(1-e^{\left(-\delta\tilde{\varepsilon}^{p}\right)}\right) \tag{2.8}$$

was fit to test data [2]. The material properties are given in Table 4.

Table 4: Material Properties for Circular Bar

Shear Modulus, μ	80.1938 GPa
Bulk Modulus, K	164.206 GPa
Initial Yield Strength $Y\big\|_{\tilde{\varepsilon}^{p}=0}$	0.45 GPa
Saturation Yield Strength, Y_{∞}	0.715 GPa
Linear Hardening Coefficient, H	0.12924 GPa
δ	1.5

The experimental data published in [**Error! Reference source not found.**] is given in Figure 7.

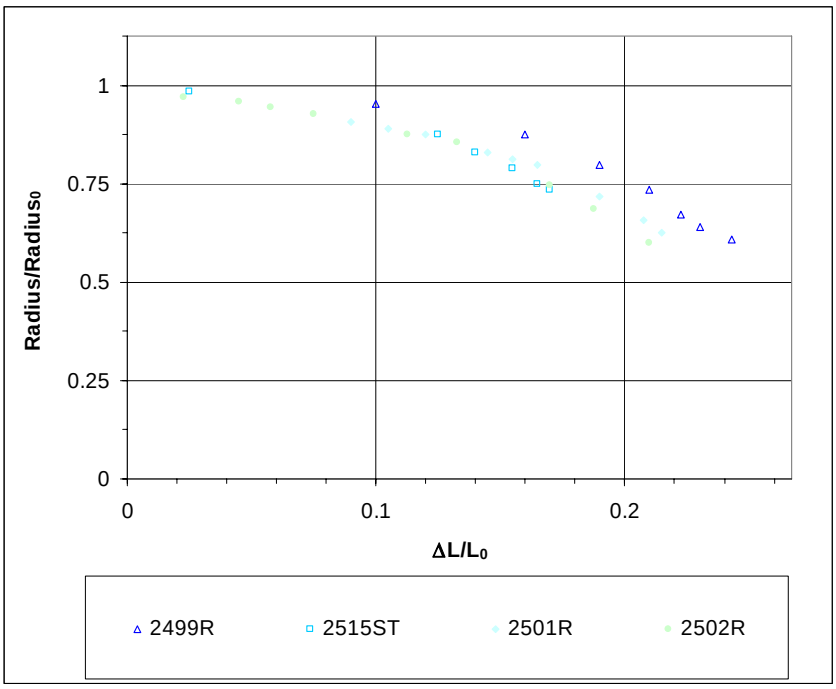

Figure 7: Necking of a Circular Bar

2.3.2 Ball Forging

A common process for manufacturing of balls is by forging a cylindrical billet between two dies with hemispherical sockets. Experimental data for the 1100 billet with 1070 carbon steel dies was reported in [21]. The radius of the aluminum billet is 12.4 mm with a height of 18.171 mm. The radius of the hemispherical socket of the die is 7.938 mm. Hardening data was fit with a nonlinear isotropic hardening law given in (2.8). Material properties of the aluminum 1100 are summarized in Table 5.

Table 5: Material Properties for Ball Forging

Elastic Modulus, E	13,000 MPa
Poisson's Ratio, ν	0.3
Initial Yield Strength $Y\big\|_{\tilde{\varepsilon}^p=0}$	65.0 MPa
Saturation Yield Strength, Y_∞	96.0 MPa
Linear Hardening Coefficient, H	41.8 MPa

δ	16.0

Figure 8 depivts the hardening data for the aluminum 1100 and the nonlinear fit to the data.

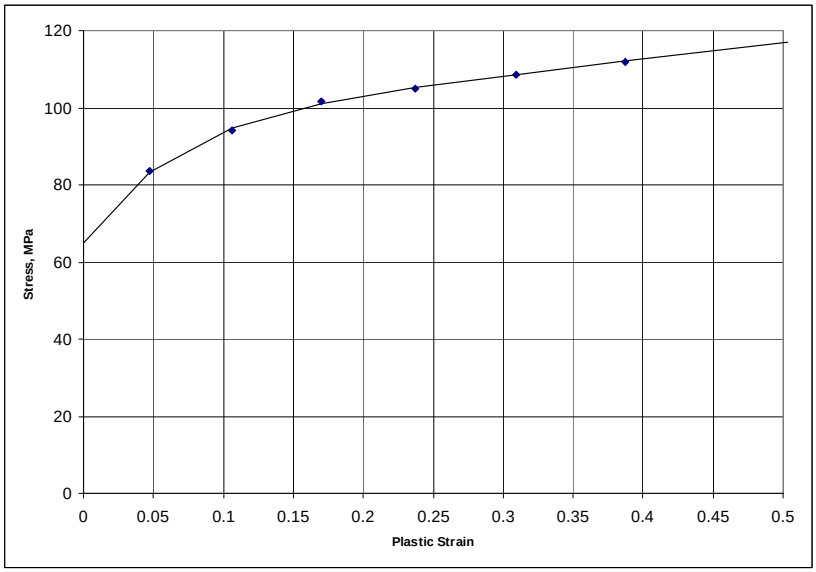

Figure 8: Aluminum 1100 Hardening Data with Nonlinear Fit

The initial geometry of the forging process is shown in Figure 10.

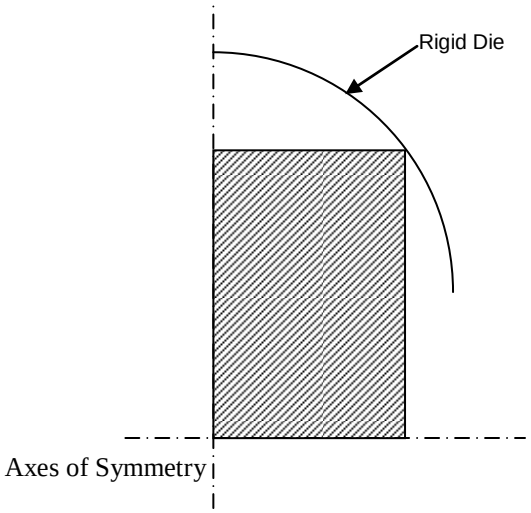

Figure 9: Axisymmetric Geometry of Ball Forging

The forging force versus displacement is given in Figure 10. Initially, there is nearly linear growth of force versus displacement. However, near the end of the process, when the billet is highly constrained, the forging force increases significantly.

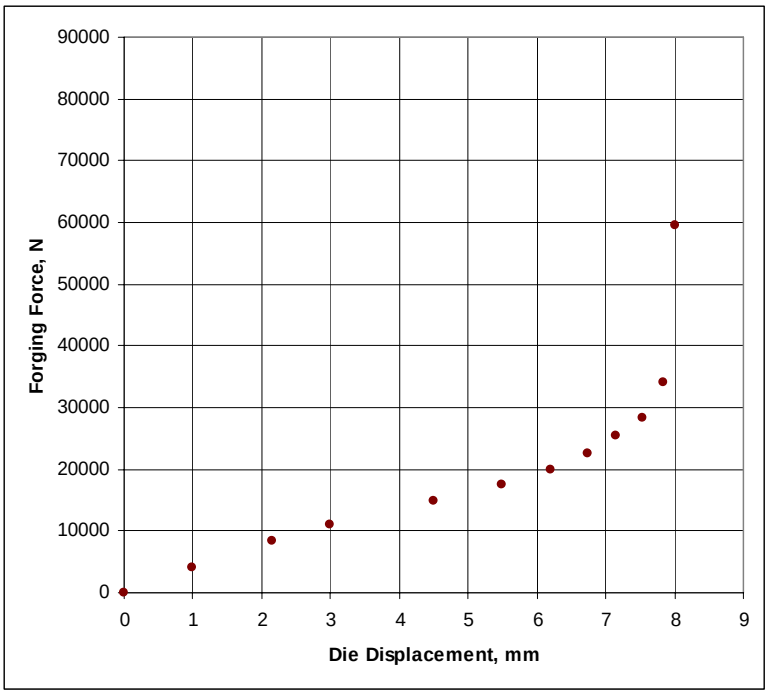

Figure 10: Experimental Forging Force vs. Die Displacement for Ball Forging

2.3.3 Upsetting of Billet

Experimental results of the upsetting of an aluminum 1100 billet constrained between two dies with cylindrical sockets were reported in [21]. The dimensions are given in Figure 11. The nonlinear isotropic hardening law and material parameters defined in Table 5 are used.

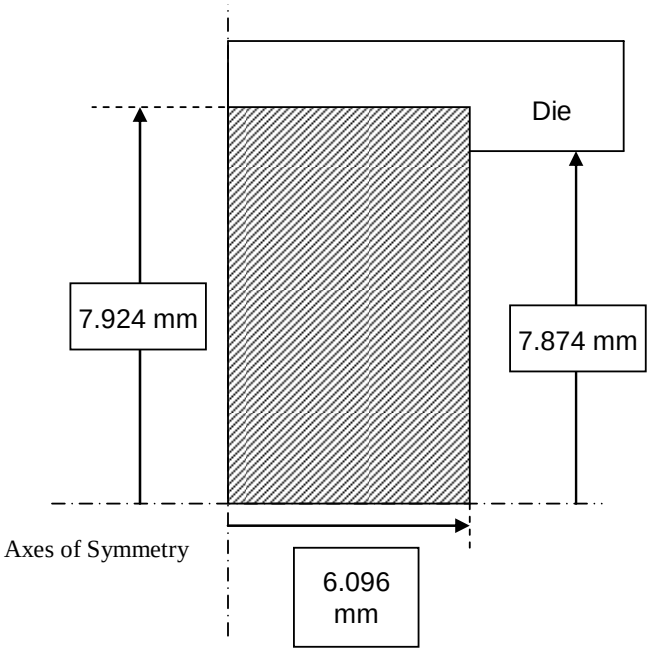

Figure 11: Initial Geometry of Billet

The experimental force-displacement results are plotted in Figure 12.

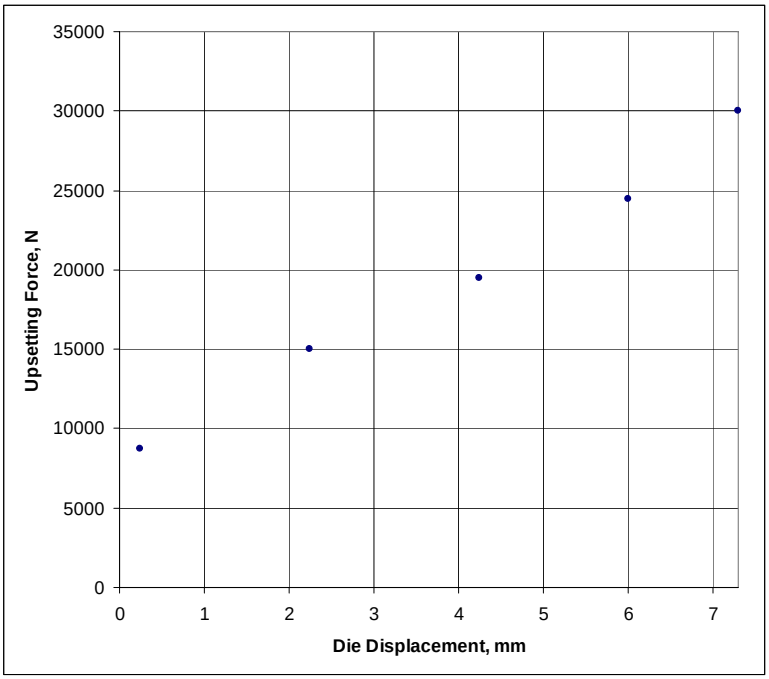

Figure 12: Experimental Force to Upset Aluminum Billet

3. PERFORMANCE IN OBSTACLE TEST

In this section we report performance studies of two hypoelastic algorithms (employing Jaumann and Green-Naghdi [5] objective stress rates), and the two hyperelastic algorithms (Simo et. al. [8, 9,10] and Eterovic and Bathe [11]) in the proposed obstacle.

3.1 Performance in the Qualitative Verification Tests

3.1.1 Simple Shear

Figures 13-16 show the results in a simple shear test. All four models considered predict similar stress response for isotropic hardening. The oscillatory behavior of the Jaumann objective stress rate with linear kinematic hardening is not consistent with experimental data as originally suggested by Nagtegaal [12]. The Green-Naghdi algorithm does not exhibit the oscillatory behavior for the linear kinematic hardening, but the value of the stress monotonically increases up to infinity. Somewhat surprising is that hyperelastic Eterovic and Bathe formulation shows oscillatory response essentially tracking the Jaumann formulation. The Simo algorithm shows an anomaly of nonzero σ_{33}. The results of all four algorithms have some inconsistencies with experimental observations outlined in previous Section: shear stress should be bounded and non-oscillatory; the peak axial stress, σ_{22}, does not occur at the peak shear stress as observed.

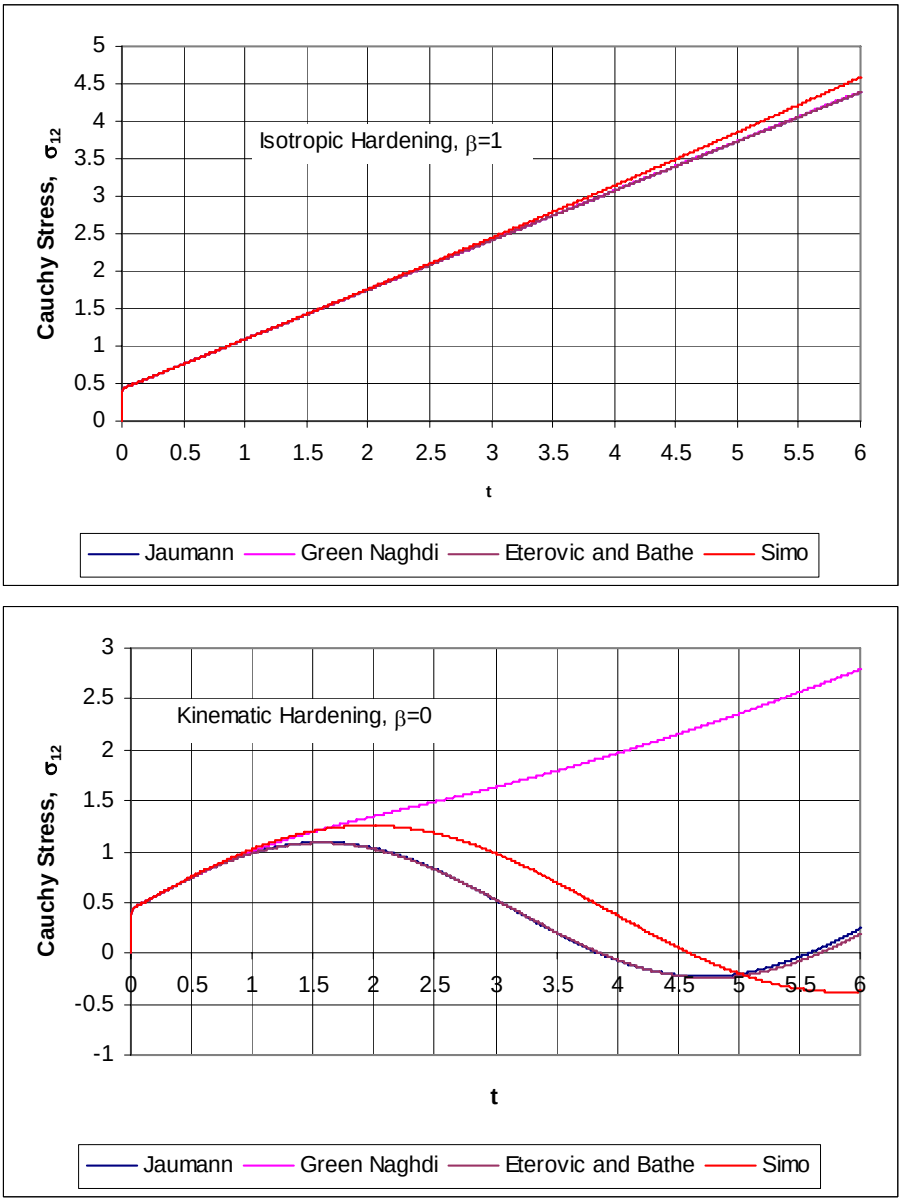

Figure 13 σ_{12} Results for Simple Shear

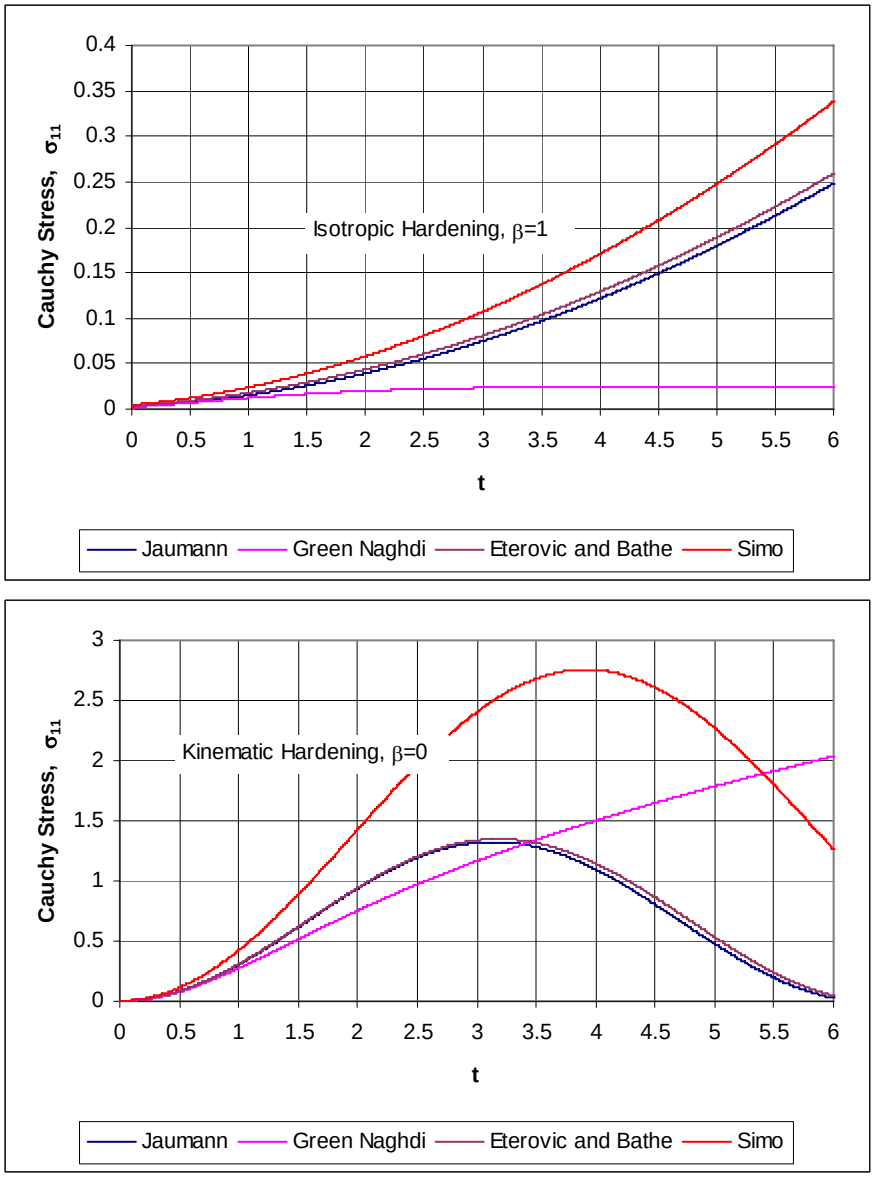

Figure 14 σ_{11} Results for Simple Shear

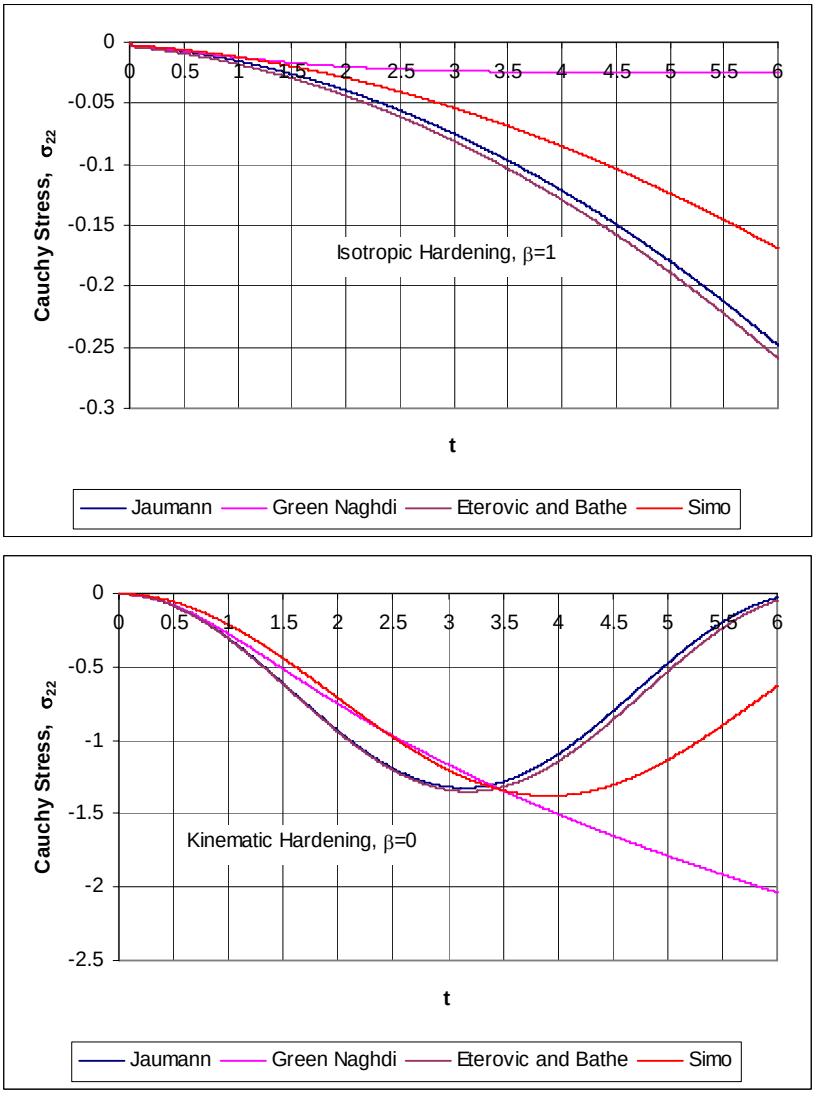

Figure 15 σ_{22} Results for Simple Shear

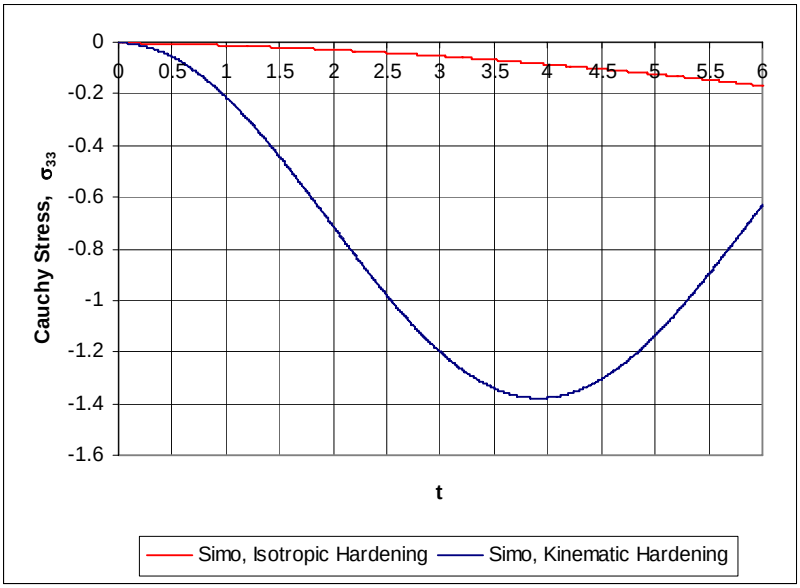

Figure 16 σ_{33} Results for the Simple Shear using Simo Algorithm

For linear kinematic hardening, two simple hypoelastic algorithms were studied. For simple shear deformation, polar decomposition of the incremental deformation gradient is used to construct the incremental rotation tensor. For the second algorithm, polar decomposition of the total deformation gradient was used to obtain the total rotation tensor. The total rotation tensor is used to update the rotational component of stress. The stress value from the previous increment is rotated back to the initial configuration using the rotation tensor from the previous increment and then the total current rotation tensor is used to update the rotational component of the stress update. Figures 17 and 18 display the stress results of this simple algorithm. Oscillatory behavior is predicted using the incremental rotation algorithm and unbounded monotonic behavior is predicted by the total rotation algorithm, similarly with the results obtained using Jaumann and Green-Naghdi objective rates, respectively. This is not surprising, since the Jaumann and Green-Naghdi objective rates coincide with the corresponding incremental rotation updates as the size of the increment approaches zero.

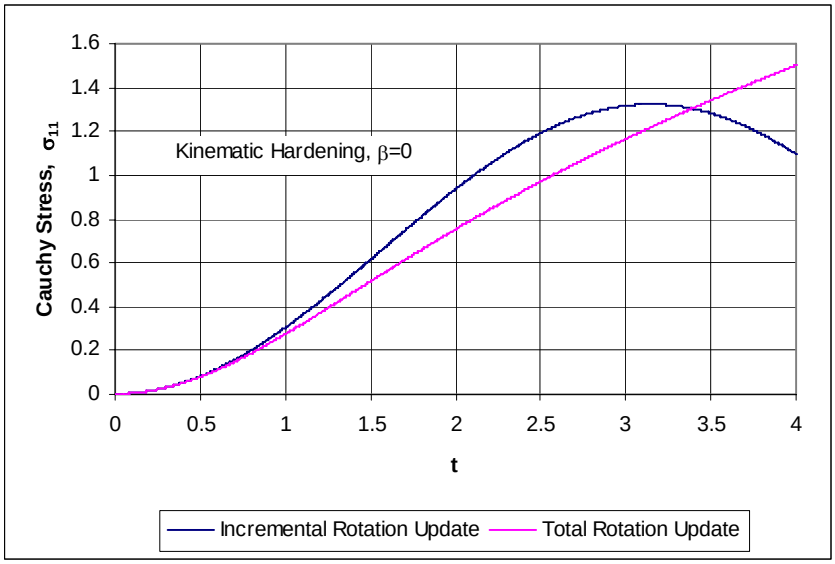

Figure 17 σ_{11} Results of the Incremental and Total Rotation Updates

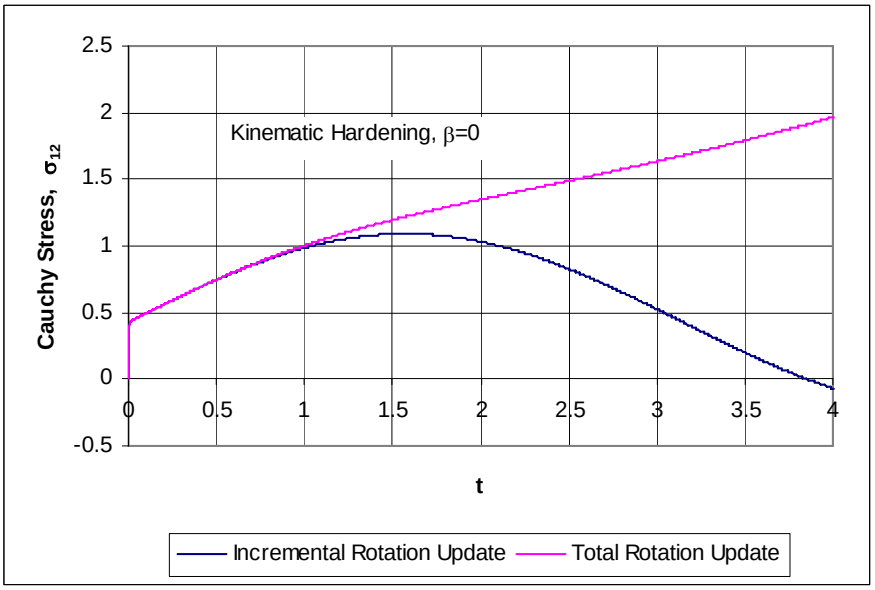

Figure 18 σ_{12} Results of the Incremental and Total Rotation Updates

3.2 Performance in the Qualitative Verification Tests

3.2.1 Expansion of a Thick-Walled Cylinder

Results of the thick-walled cylinder test problem, as defined in the previous section, are shown

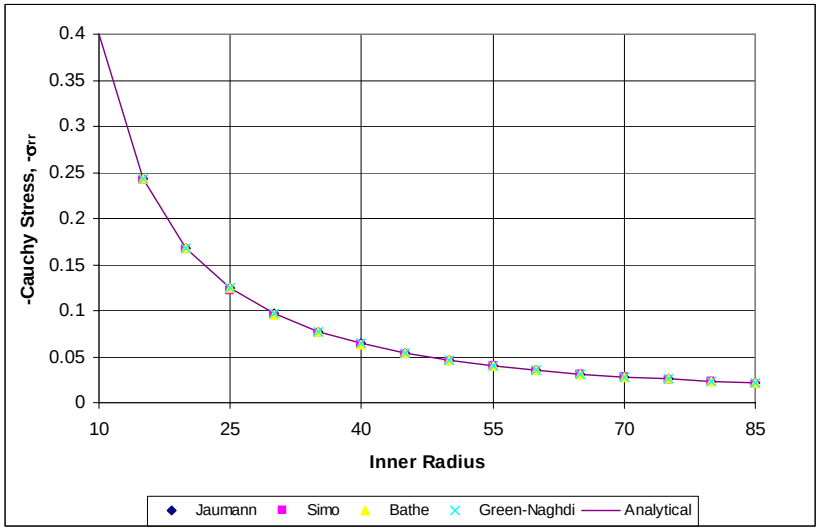

Figure 19: Inner Boundary Cauchy Radial Stress, σ_{rr}, vs. Inner Radius

in Figure 19. It can be seen that all algorithms produce nearly identical results with the maximum percentage difference being on the order of 2%. This is not surprising since both rotations and elastic strains are small.

3.2.2 Expansion of a Thick-Walled Sphere

The results of the thick-walled cylinder test problem, as defined in the previous Section, are shown in Figure 20 as pressure versus porosity of the sphere.

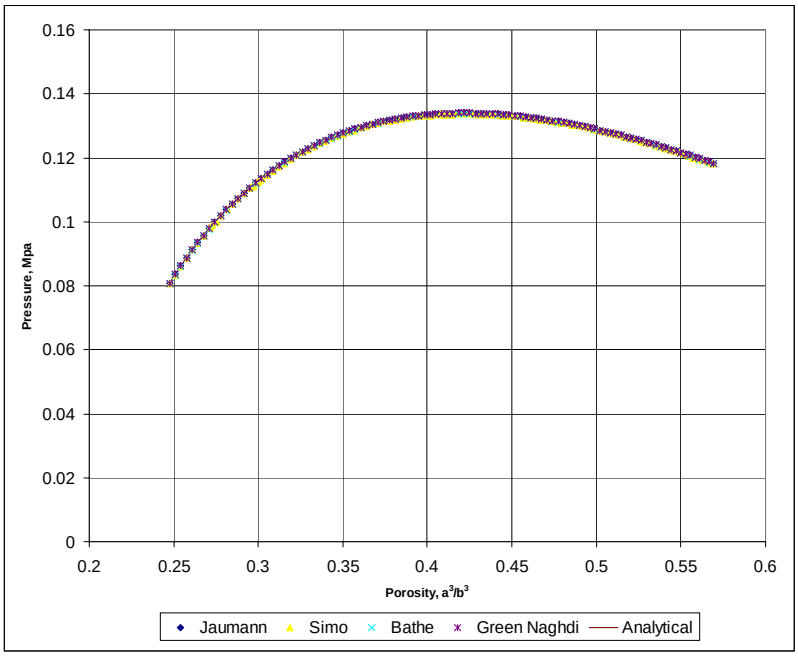

Figure 20: Internal Pressure vs. Porosity for Thick-Walled Sphere

It can be seen that the results of all algorithms are in good agreement with the reference analytical solution.

3.3 Performance in Validation Tests

3.3.1 Necking of Circular Bar

The deformed geometry of the circular bar test problem, as defined in Section 2.3.1, is shown in Figure 21. The reduction in radius versus nominal strain is given in Figure 22.

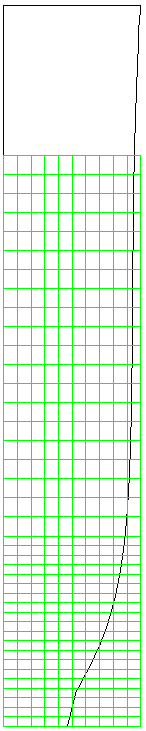

Figure 21: Initial and Deformed Geometry of Circular Bar

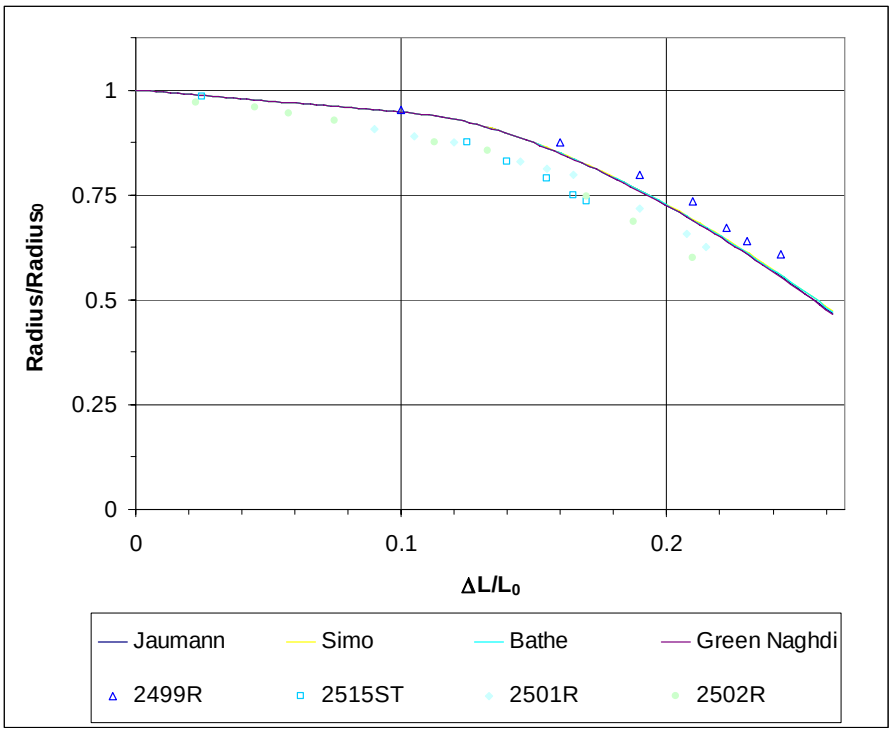

Figure 22: Reduction in Radius for Necking Circular Bar

It can be seen that all algorithms are match up very well with the experimental data published in [**Error! Reference source not found.**].

3.3.2 Ball Forging

The axisymmetric mesh of the billet and the deformed geometry after the forging process defined in Section 2.3.2 are shown in Figure 23.

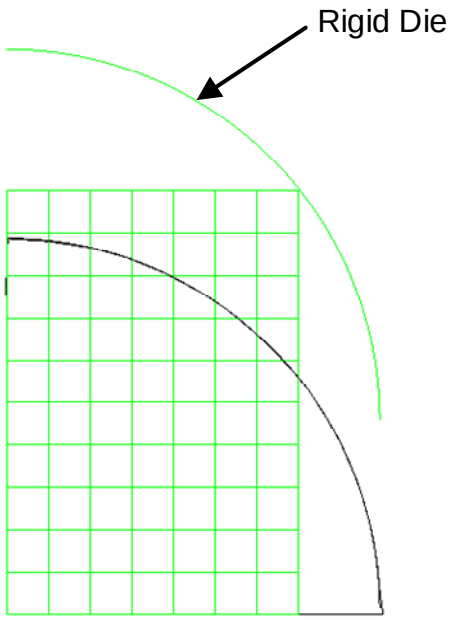

Figure 23: Initial and Deformed Geometry of Ball Forging

The results of the finite element models are plotted with experimental data in Figure 23. The nearly linear growth of force versus displacement is predicted well by each model. However, near the end of the process, when the billet is highly constrained the error substantially increases. A portion of this error is probably due to the use of rate independent plasticity. The plastic strain rate increases significantly in the last stages of the forging process.

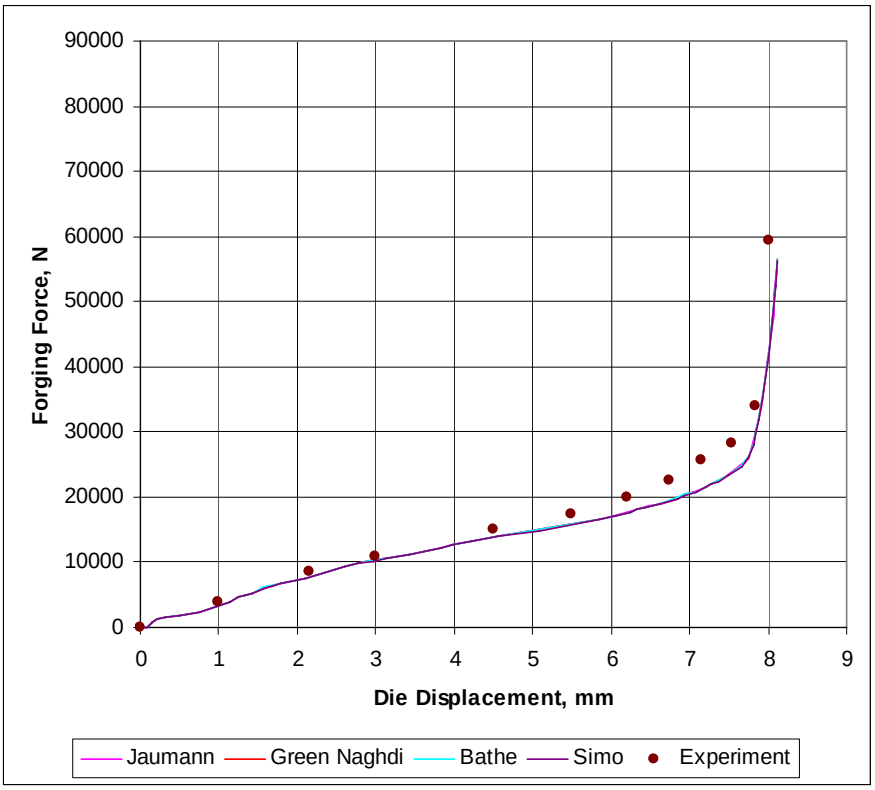

Figure 24: Forging Force vs. Die Displacement for Ball Forging

3.3.3 Upsetting of Billet

The deformed geometry of the billet undergoing upsetting as defined in Section 2.3.3 is given in Figure 25.

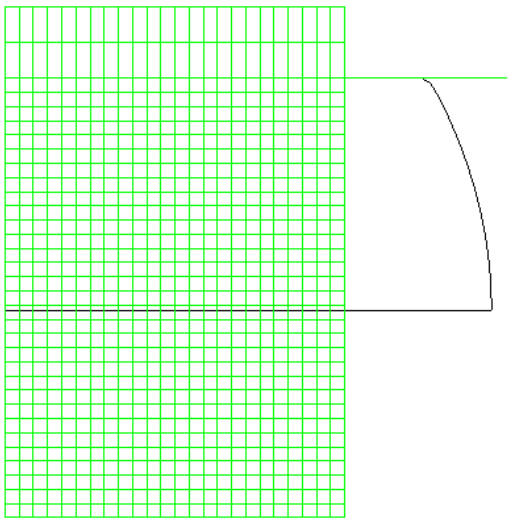

Figure 25: Initial and Deformed Geometry of Billet

The results of the models considered are plotted against experimental data in Figure 26. The general trend of the force versus displacement curve is predicted well, but the magnitude of the force predicted by all for models is about 10% less than the experimental value. The process was performed at a constant upsetting speed, thus the strain rate increases throughout the process.

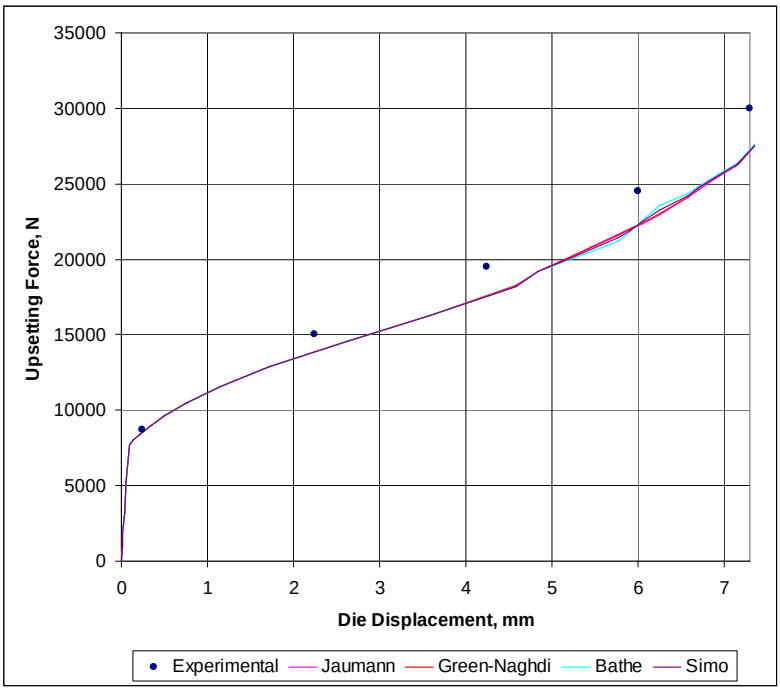

Figure 26: Force to Upset Aluminum Billet

4. CONCLUSIONS AND FUTURE RESEARCH

An obstacle test for large deformation plasticity problems is proposed for evaluation of common mathematical models and numerical algorithms. The obstacle test consists of three categories of test problems: (i) qualitative verification, (ii) quantitative verification and (iii) validation. The algorithms tested performed reasonably well except for the simple shear problem were certain anomalies were identified.

The obstacle test could be expanded to address the following issues: (i) identification of sources of error and (ii) computational efficiency. The obstacle test presented here does not provide any information on the sources of error; whether it is due to material response, large rotations, decomposition of elastic and inelastic response; etc. Test problems perhaps can be engineered so that only one parameter is varied at a time. To our knowledge, experimental data supporting such an approach does not exist today. The major two factors affecting computational efficiency are: (i) cost of consistent (or not) linearization and stress update, and (ii) the size of the load increment required for maintaining sufficient accuracy of the stress

update algorithm. This type of analysis would permit benchmarking of cost versus accuracy for various models and algorithms considered.

5. References

1. Truesdell, C and W Noll, *The Nonlinear Field Theories*, 1965, Springer-Verlag, Berlin

2. Simo, JC and TJR Hughes, *Computational Inelasticity*, 1998, Springer-Verlag, New York

3. Belytschko, T, WK Liu, and B Moran, *Nonlinear Finite Elements for Continua and Structures*, 2003, John Wiley & Sons

4. Simo, JC and KS Pister, "Remarks on Rate Constitutive Equations for Finite Deformation Problems: Computational Implications," *Computer Methods in Applied Mechanics and Analysis* **46** (1984), 201-215

5. Dienes, JK, "On the Analysis of Rotation and Stress Rate in Deforming Bodies," *Acta Mechanica* **32** (1979), 217-232

6. Hughes TJR and J Winget, "Finite Rotation Effects in Numerical Integration of Rate Constitutive Equations Arising in Large Deformation Analysis," *International Journal for Numerical Methods in Engineering* **15** (1985), 1862-1867

7. Lee EH, "Elastic-Plastic Deformations at Finite Strains," *Journal of Applied Mechanics* **36** (1969), 1-6

8. Simo, JC and M Ortiz, "A Unified Approach to Finite Deformation Elastoplasticity Based on the use of Hyperelastic Constitutive Equations," *Computer Methods in Applied Mechanics and Analysis* **49** (1985), 201-215

9. Simo, JC, "A Framework for Finite Strain Elastoplasticity Based on Maximum Plastic Dissipation and the Multiplicative Decomposition: Part I. Continuum Formulation," *Computer Methods in Applied Mechanics and Analysis* **66** (1988), 199-219

10. Simo, JC, "A Framework for Finite Strain Elastoplasticity Based on Maximum Plastic Dissipation and the Multiplicative Decomposition: Part II. Computational Aspects," *Computer Methods in Applied Mechanics and Analysis* **68** (1988), 1-31

11. Eterovic, AL and KJ Bathe, "A Hyperelastic-based Large Strain Elasto-Plastic Constitutive Formulation with Combined Isotropic-Kinematic Hardening Using the Logarithmic Stress and Strain Measures," *International Journal for Numerical Methods in Engineering* 30 (1990), 1099-1114

12. Nagtegaal, JC and JE deJong, "Some Aspects of Non-Isotropic Work Hardening in Finite Strain Plasticity," in: EH Lee and RL Mallet, eds., *Plasticity of Metals at Finite Strains: Theory, Experiment, and Computation,* Proceedings of Research Workshop, Stanford University (1981), 65-102

13. Montheillet, F et. al., "Axial Stresses and Texture Development During the Torsion of Al, Cu, and α-Fe," *Acta Metallurgica* **32** No. 11 (1984), 2077-2089

14. Swift, HW, "Length Changes in Metals Under Torsional Overstrain," *Engineering* 163 (1947), 253-257

15. Weber, G and L Anand, "Finite Deformation Constitutive Equations and a Time Integration Procedure for Isotropic, Hyperelastic-Viscoplastic Solids," *Computer Methods in Applied Mechanics and Analysis* **79** (1990), 173-202

16. Hoger, A, "The Stress Conjugate to Logarithmic Strain," *International Journal of Solids and Structures* **23** (1987), 1645-1656

17. Dafalias, YF, "Plastic Spin: Necessity or Redundancy?" *International Journal of Plasticity* **14** (1998) 909-931

18. Montans, FJ and KJ Bathe, "Computational Issues in Large Strain Elasto-Plasticity: an Algorithm for Mixed Hardening and Plastic Spin," *International Journal for Numerical Methods in Engineering* (2005) in press

19. Lubliner, J, *Plasticity Theory*, 1990, Macmillan, New York

20. Carroll, MM, "Radial Expansion of Hollow Spheres of Elastic-Plastic Hardening Material," (1985)

21. Shih, AJM, and HTY Yang, "Rate Dependent Metal Forming Processes," *International Journal for Numerical Methods in Engineering* **31** (1991)

22. ABAQUS V6.5, ABAQUS Inc.

23. ASME PTC#60 "Guide for Verification and Validation in Computational Solid Mechanics" ASME, Draft 2/23/05.